Construction and Building Materials 155 (2017) 770–779

Contents lists available at ScienceDirect

Construction and Building Materials

journal homepage: www.elsevier.com/locate/conbuildmat

Waterproof ultra-high toughness cementitious composites containing nano reservoir silts

Hedong Li, Shilang Xu *, Qiang Zeng *

Institute of Advanced Engineering Structures and Materials, College of Civil Engineering and Architecture, Zhejiang University, Hangzhou 310058, PR China

HIGHLIGHTS

- A waterproof cementitious composite was designed and fabricated.
- The toughness of cementitous composites was maintained by the dosage of nano reservoir silts upto 5%.
- The water absorption and penetration of cementitous composites were depressed essentially.
- The good material properties of waterproof cementitious composites facilitate their uses.

GRAPHICAL ABSTRACT

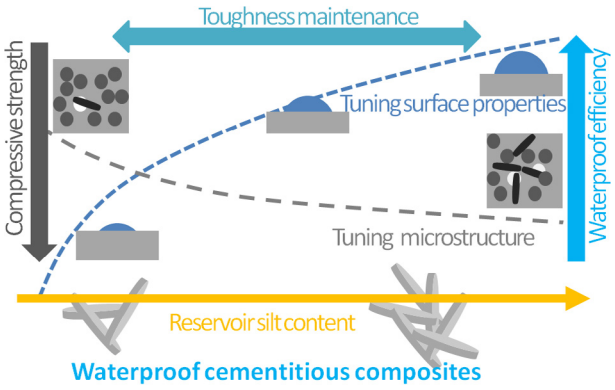

ARTICLE INFO

Article history:
Received 21 April 2017
Received in revised form 5 August 2017
Accepted 19 August 2017

Keywords:
Waterproof
Composite
Microstructure
Nano particle

ABSTRACT

The waterproof ability of cementitious composites is essentially important for the uses in the aspects of construction, decoration and repair. Here we reported a waterproof ultra-high toughness cementitious composite (WUHTCC) that has the function of seepage resistance. The waterproof effect was improved by incorporating nano reservoir silts (NRSs) into the binders of WUHTCC. The mechanical properties, microstructures and water resistances of the WUHTCCs with different loadings of NRSs were tested to assess the affecting factors. The results show that increasing the loadings of NRSs maintains and/or enhances the toughness of WUHTCCs, but decreases the compressive strength. The water absorption is decreased, and the penetration pressure and time are increased significantly with increasing the NRS content. While the incorporation of NRS particles into cementitious matrix leads to a slight increase of porosity, it shows no significant changes of micro morphology. The variations of the mechanical and waterproof properties of WUHTCCs are induced by the hydrophobic and sheet-like NRS particles that alter the surface properties and microstructures of the material substrate. The WUHTCCs with good material properties developed in this study for seepage control facilitate their applications in the fields of construction, decoration and repair.

1. Introduction

Most cementitious materials (cement paste, mortar and concrete) have relatively low permeability, however, the problems of water seepage always occur in the roofs, bathrooms and basements of buildings, the segments of tunnels, and the stations of metros

* Corresponding authors.
E-mail addresses: lihedong@zju.edu.cn (H. Li), slxu@zju.edu.cn (S. Xu), cengq14@zju.edu.cn (Q. Zeng).

http://dx.doi.org/10.1016/j.conbuildmat.2017.08.119
0950-0618/

[1]. A traditional method for mitigating water seepage is to apply an organically or inorganically waterproof coating on the material surface. While this method may be effective, the high volatile organic compound level is harmful to humans and the waterproof function of this coating layer may fade rapidly under aggressive environments, such as, external loads, UV exposing, heating, wetting and drying and freezing and thawing [2–5]. Furthermore, an elaborate primer is generally needed for the favorable performance of a waterproof coating, which increases the costs of economy and manpower. So it is always a challenge to find an easy-to-use, manpower saving and durable way or material to control the water seepage of buildings and infrastructures. Cementitious composites modified by fibers and nano additives, like ordinary cement mortar and concrete, can adhere to most natural and man-made building materials without specifically elaborate pretreatments [6], which may pave an alternative path to control the water seepage problems of buildings and infrastructures.

To date, numerous studies have been conducted to investigate the effects of clay-based nano additives on mechanical and transport properties of cementitious materials. Chang et al. [7] studied the mechanical properties and water permeability of Portland cement paste with nano montmorillonite, and found that the positive effect of the nano clay was in a limited loading range. Kafi et al. [8] reported the positive effect of nano montmorillonite on the mechanical properties of paste and mortar in a broader loading range. Hakamy et al. [9] investigated the mechanical property and water absorption of nano clay and calcined nano clay-cement composites, and found an obvious decrease of water absorption by the nano clays. Similar studies on the enhancement of mechanical properties of cementitious materials by nano clays have been extensively reported [10–13]. Based on systematically experimental studies, Kuo and coworkers [14–17] suggested that the design strength for normal-strength cement mortars can be attainable for up to 30% replacement of fine aggregates by surface-modified nano reservoir silt (NRS) particles that generally show layered nano structures and are mostly composed of SiO_2, Al_2O_3 and Fe_2O_3, and the permeability of the materials can be essentially decreased. The hydrophobic nano clays are expected to inhibit water from entering capillary pores and the space between the layered nano clays, and in consequence, the water permeability is lowered [18].

It is noteworthy that the relatively brittle feature of ordinary Portland cement mortar and concrete, although modified by nano clays, limits their uses. Fiber-reinforced ultra-high toughness cementitious composites (UHTCCs), under rational design, can show excellent toughness, impact resistance and durability [19–22] which thus provides good substrates to design and fabricate the cementitious composites with the functions of cracking and seepage controls. Hakamy et al. [23–25] reported a type of NaOH treated hemp fabric and nano clay-reinforced cementitious nanocomposites with good mechanical and durability. The improvement of mechanical properties of cementitious composites by nano clays and fibers has been reported extensively [26,27]. Recently, Yu et al. [2] reported a type of waterproof engineered cementitious composites (WECCs) containing a waterproof admixture for seepage control. It was found that the water absorption of WECCs was greatly decreased [2]. This thus throws fresh light on the design and fabrication of waterproof cementitious composites by incorporating surface-modified nano clays into cementitious binders to control water seepage.

Inspired by the work of waterproof cement mortars by Kuo et al. [14–17] and the previous studies of UHTCCs in our institute [28–30], here we reported a type of waterproof ultra-high toughness cementitious composites (WUHTCCs), where the loadings of NRS particles used are in a relatively broad range. Comprehensively experimental measurements of WUHTCCs with indepth analyses allow exploring the affecting factors and mechanisms accounting for the decrease of compressive strength, the maintenance of toughness, and the enhancement of waterproof. The findings of this research are expected to optimize the design of WUHTCCs and to pave a wild path for the uses of the materials in construction, decoration and repair with auxiliary seepage control.

2. Experimental programme

2.1. Materials and mixture design

The WUHCCs designed and fabricated in the present study are based on a UHTCC with strain hardening behaviors developed by the same research group (e.g., [19,20,28–30]). To achieve the rapid hardening of WUHTCCs, which is potentially used for emergency repair, a rapid hardening cement classified as P.II 52.5R according to the Standard of GB175-2007 (China) [31] was used for fabricating the WUHTCC matrix. The binders also included active fillers (AF) that contain fly ash and silica fume. A silica sand (SS) was used as an inactive filler; see Table 1 for detailed mixture proportions. The detailed physical properties of the binders can be found elsewhere [2]. A very high volume of fillers (i.e., AF and SS) other than cement clinkers based on a green UHTCC mix as reported in Refs. [19,20,28–30] shows beneficial effects to the reduction of steady state crack width, waterproofing and the long-term durability of a UHTCC structure. A water-to-powder ratio of 0.326 was used, and a polycarbonate super-plasticizer (SP) was added to control the rheology of flesh WUHTCCs. Discontinuous PVA fibers (K-II REC15, Kuraray Co., Ltd) in the volume fraction of 2% were used to enhance the toughness of cementitious composites. The average length, diameter, density, elastic modulus and strength of the PVA fibres are 12 mm, 39 μm, 1.30 g/ml, 16.9 GPa and 1.28 GPa, respectively. To tune the waterproof efficiency of UHTCC, a commercial nano reservoir silt (NRS) powder (Lotos, Techome Technology Co. Ltd) was added into the binders. The main components of NRS particles are quartz (around 30%), smectite or montmorillonite (around 60%) containing SiO_2, Al_2O_3 and Fe_2O_3 and other phases (around 10%). A cation-exchange reaction method was used to modify the surface properties of NRS particles [14,15]. The NRS particles are thin warped plates with the mean diameter within 10 to 50 μm and the mean thickness lower than 100 nm; see Fig. 1. The NRS-to-binder ratios of 0%, 1%, 2% and 5% were designed to obtain different WUHTCC mixes, namely, WUHTCC-0, WUHTCC-1, WUHTCC-2 and WUHTCC-5, respectively; see Table 1.

All binders as well as NRS powders in the proportions presented in Table 1 were carefully poured into a mixer (Hobart HL200), and were mixed for 60 s to avoid the possible heterogeneity of the raw materials due to different densities. Later, the precisely weighed water was added into the mixer, and then a rapid mix lasting for 3 min was conducted. After that, the PVA fibers were added into slurries with further 3-min mixing. The mixed slurries were cast in greased steel molds with short-time vibrations. A polyethylene sheet was used to cover the surfaces exposed after the surface finishing step. This prevents the possible damages of the WUHTCC specimens induced by moisture loss. The specimens were placed in a chamber under room temperature for 24 h prior to demolding. After demolding, all specimens were cured up to 28 days in a room with the temperature and relative humidity controlled at $20 \pm 2\,^{\circ}C$ and $> 95\%$, respectively. Different specimens were prepared for different tests. Specimens in cuboid of $100 \times 100 \times 400\ mm^3$ were prepared for four-point bending (FPB) test. Cubic specimens with dimensions of $70\ mm^3$ were prepared for the tests of compressive strength and water absorption. Conic specimens with upside and underside surface diameters of 70 mm and 80 mm, height of 30 mm were prepared for water penetration test. The damaged specimens from the compressive strength and FPB tests were crushed into small pieces for pore structure and microstructure tests.

2.2. Microstructural analysis

For pore structure measurement, we employed a mercury intrusion porosimetry (MIP) (Autopore IV 9510, Micromeritics Instrument Corporation, Norcross, GA, USA). The measurement of MIP can provide the pore structure and material informations of samples (e.g., porosity, mean and medium pore sizes, and pore size distribution). The mercury intrusion and extrusion were performed with the pressure from 3.7 kPa to 414 MPa with the equilibrium time for each applied pressure level of 10 s. For the evaluation of the pore size distributions of the WUHTCC samples, the contact angle between mercury and pore surface and the surface tension between vapor and liquid mercury were set as 130° and 485 N/m respectively [32,33]. The intrusion-extrusion hysteresis [34,35] was not considered in this study.

The micro morphology of WUHTCCs was observed and analysed using an FEI Quanta FEG650 field emission environmental scanning electronic microscopy (ESEM). The samples for ESEM analysis were prepared from the crushed specimens after mechanical tests. In order to preserve the original topography of fracture surfaces, all the samples were only cut into an appropriate size without polishing the observation surfaces. The accelerating voltages within 10 kV to 20 kV were used,

Table 1
Mix proportions of WUHTCCs in reference to the total weight of powders. RHC: Rapid hardening cement, AF: Active filler, SS: Silica sand, NRS: Nano reservoir silt, SP: Polycarbonate superplasticizer, PVA: Kuraray K-II REC15 polyvinyl alcohol fiber, W: Water, B: Binder and P: Powder.

Mix ID	Powder				NRS/B	SP/P	PVA	W/P
	Binder							
	RHC	AF	SS	NRS				
WUHTCC-0	0.200	0.600	0.200	0	0%	0.25%	2%vol	0.326
WUHTCC-1	0.200	0.592	0.200	0.008	1%	0.25%	2%vol	0.326
WUHTCC-2	0.200	0.584	0.200	0.016	2%	0.25%	2%vol	0.326
WUHTCC-5	0.200	0.561	0.200	0.039	5%	0.25%	2%vol	0.326

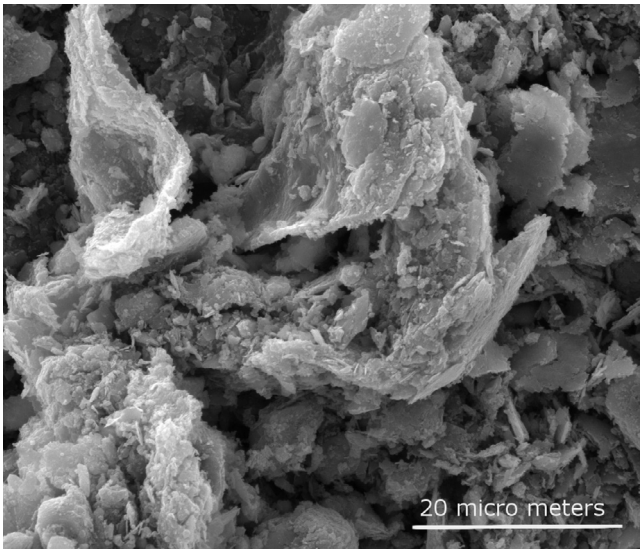

Fig. 1. Micro morphology of sheet-like nano reservoir silts.

because the higher voltages may damage the microstructure of the samples, while a lower voltage may lead to grainy results [36]. The working distances were in the range of 15 mm to 35 mm and the spot was controlled as 3.

2.3. Mechanical measurement

A compression test was used to assess the strength of cubic WUHTCC specimens. The compression test was operated with a 25 kN Instron full-functional test machine. By aid of its electro-hydraulic servo system, the loading rate was maintained at 0.3 MPa/s. A spherical bearing was installed between the specimen and lower loading head to keep uniaxial loading. The load was measured by a force sensor attached to the upper loading head. As the test proceeded, the forces were recorded, and the maximum values were adopted to calculate the compressive strength.

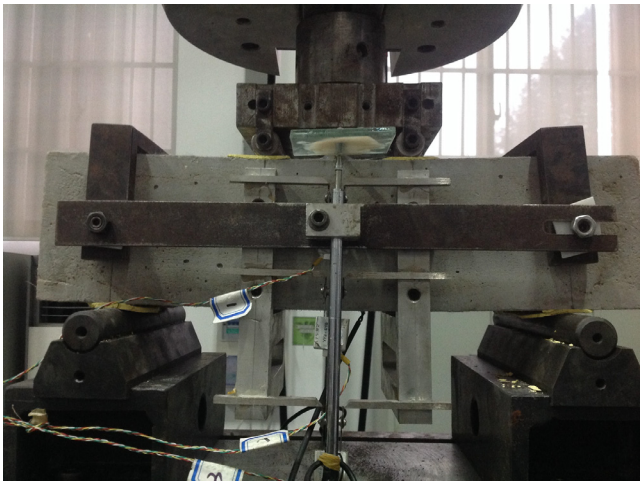

Fig. 2. An *in-situ* image of an FPB test.

An FPB test was employed to assess the toughness of WUHTCCs; see Fig. 2. The machine used was the same to the compression test. Before testing, the WUHTCC specimens were loaded in a home-made steel frame with LVDT meters for the measure of mid-span deflection. The loading span was 100 mm and the support span was 300 mm. During testing, the moving speed of the loading head was maintained at 0.2 mm/min. At least 3 samples for each mix were tested. The measured data were recorded simultaneously by an integrated measurement and control system, which provides the loading-deflection curves of WUHTCC specimens.

After the FPB tests, the high resolution images of all the WUHTCC specimens were taken from the bottom surfaces by a commercial camera. An open-source software, ImageJ [37], was used to analyse the cracking patterns of WUHTCC specimens. An Otsu threshold algorithm was used to segment the cracks from the WUHTCC matrix. Then the geometric information of cracks, such as, size, roundness and distribution, can be obtained directly from the particle analysis in ImageJ. Further statistical analysis can be performed to acquire the mean or median values of a quantity (e.g., crack width). Although the Otsu threshold algorithm has been debated for its accuracy in image processing, it has been suggested that this method could, at least semi-quantitatively, characterize the cracks and/or pores of cement-based materials [38]. Here we did not consider the possible distortion effect of the 2-D images on the real 3-D spacial structures of cracks. More of the relevant content can be found in the pertinent research elsewhere [39].

2.4. Water absorption and penetration tests

12 cubic WUHTCC specimens in total were used to test their water absorption according to the criteria DL/T 5126G2001 (China) [40]; see Fig. 3(a). The initial cubic specimens (with the curing age of 28 days) were first placed in an oven with $80 \pm 2\ ^{\circ}C$ for drying. After 48 h, the specimens were transferred to a chamber, cooled to the room temperature and weighed (m_d). Then the specimens were immersed in water with $20 \pm 2\ ^{\circ}C$ for water absorption. After 48 h, the specimens were removed from the water, and the surfaces were dried by blotting papers. Once a surface-dried condition was obtained, the specimens were weighed immediately (m_s). Three independent absorption tests were performed to make sure the reproducibility and reliability of the absorption data. The absorption of WUHTCCs can be calculated as: $(m_s - m_d)/m_d$. Unlike the sorption test ASTM C 1585 [41], the water immersion test can not give the sorption rate of the specimens, however, the obtained absorption is a reliable (and at least semi-quantitative) parameter to determine the waterproof efficiency of WUHTCCs.

A water penetration test was performed to assess the waterproof efficiency of WUHTCCs according to the Standard JGJ/T 70-2009 (China) [42]; see Fig. 3(b). 6 specimens for each mixture, and 24 specimens in total, were firstly placed into steel cones. The interfacial spaces between the steel cones and the round surfaces of the specimens were sealed with wax, while both the down and up surfaces were free. During testing, a water pressure of 0.2 MPa was applied slowly to equilibrium. After 2 h, the water pressured was increased by 0.1 MPa, and the equilibrium time was controlled to be 1 h. In the Standard JGJ/T 70-2009 [42], tests must be stopped when the water pressure reached 1.5 MPa within 8 h [43]. Here we modified this test by prolonging the testing time and changed the criteria to justify the waterproof efficiency of WUHTCCs accordingly. The procedures of pressure-applying and equilibrium-keeping were processed until 3 of the 6 specimens leaked. The water-leaking pressure was recorded as P_l, and the maximum survival pressure for water penetration is $P_s = P_l - 1$. Accordingly, the time for water penetrating through the WECCs is $t_s = 10 \times P_s + 1$. Both the survival pressure and penetrating time were used to assess the waterproof efficiency of WUHTCCs.

3. Results and discussion

3.1. Pore structure and microstructure

Using appropriate interpretations the mercury intrusion measurement can provide the pore-and micro-structure information of a porous material, including the skeleton density, porosity, specific surface area, mean pore diameter, pore size distribution

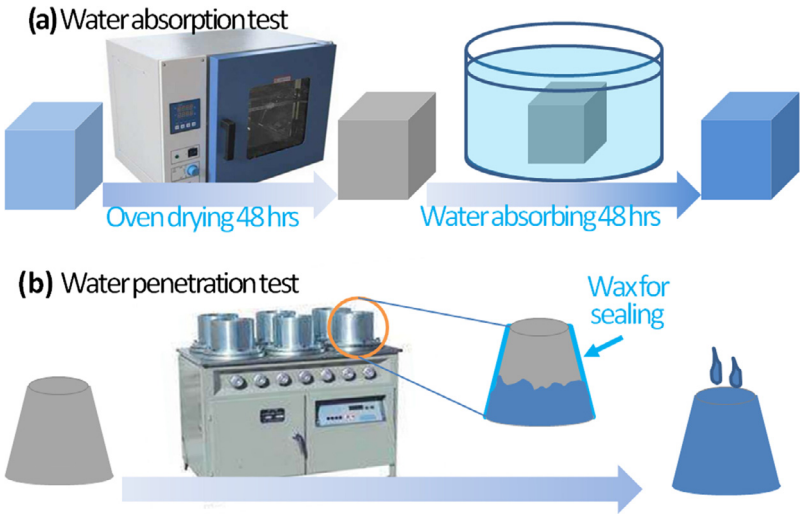

Fig. 3. Schematic illustration of water absorption and penetration tests.

and fractal dimension [44]. Fig. 4 shows the accumulative and differential pore size distributions of the WUHTCC samples. As is seen, the mercury first penetrates through a small amount of space with the size larger than 1 μm, which can be open pores, voids, cracks and/or cavities [45], then a large amount of space in the meso and micro scales < 1 μm, which can be small capillaries, gel pores and/or the confined spaces between hydrates and NRS particles. Apparently, the shapes of pore size distribution have no significant differences (Fig. 4), which tells that NRS particles have not changed the overall pore structures of WUHTCCs essentially. However, one must note that the assumption of cylindrical pores for the evaluation of pore size distribution by MIP test may cause somewhat deviations of the measured data from the real pore structure [44].

Table 2 summarizes the pore-and micro-structure properties of the WUHTCC samples extracted from the MIP tests. The average skeleton density of WUHTCCs is in the range of 2.2 to 2.3 g/ml, in accordance with the results reported in Ref. [33] despite of the different mixes. Nevertheless, the value is higher than the calculated low density (LD) C-S-H (1.44 g/ml) and high density (HD) C-S-H (1.75 g/ml) according to the Jennings C-S-H model [46], but lower than the real C-S-H globules (around 2.6 g/ml) measured by neutron and X-ray scattering techniques [47]. The limited measuring scales of the MIP technique and the different components of the hydrates of WUHTCCs from the pure C-S-H may account for the density differences. The results of MIP porosity reveal that around one third of the WUHTCC volumes are pores; see Table 2. The NRS additive seems to augment the total porosity of WUHTCCs, but the augmenting extents are very limited. This suggests that the microstructure of WUHTCCs becomes looser when NRS particles are used. This conclusion was also evidenced by the experimental results obtained in Ref. [16], where the authors reported that the total volume of accessed pores is increased as the loading of NRS particles is higher than 0.5%. Both the pore area and the median pore size of WUHTCCs have no appealing relationships with the loading of NRS particles; see Table 2. Note that the pore area and the median pore size of WUHTCCs may be, again, biased by the assumption of cylindrical pores [44] as the spaces between the sheet-like NRS particles and the WUHTCC hydrates are rather complex.

The fractal dimension of WUHTCCs based on an assumption of self-similar structures repeated in limited measuring scales was also evaluated [44]. Generally, there are two fractal regions from the MIP data of cementitious materials [48–50], i.e., the micro

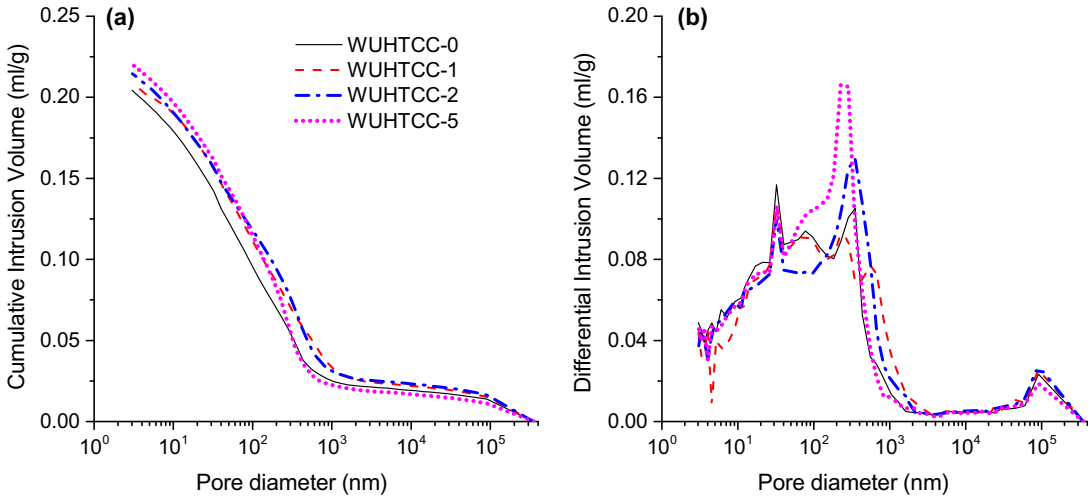

Fig. 4. The (a) cumulative and (b) differential pore size distributions of WUHTCCs from the intrusion phase of MIP test.

Table 2
The pore-structural characteristics of WUHTCCs.

Sample	Skeleton density (g/ml)	Porosity (%)	Pore area (m^2/g)	Median pore $4V/A$ (nm)	Fractal dimension (–)
WUHTCC-0	2.231	32.18	32.27	25.4	2.704
WUHTCC-1	2.228	32.31	26.36	31.7	2.748
WUHTCC-2	2.324	33.28	29.76	28.9	2.769
WUHTCC-5	2.306	33.73	31.10	28.4	2.759

fractal region resulted from the complex natures of hydrates and nano additives, and the macro one from the spacial packings of clinkers and fillers. Here we only considered the micro fractal dimensions as we were more concerned about the microstructures and the interactions between the hydrates and the NRS particles in WUHTCC matrix. Table 2 shows the fractal dimensions of WUHTCCs from the MIP tests. The fractal dimensions are in the range of 2.70 to 2.77, which are comparable with the data reported in Refs. [48,49,51]. It shows that the fractal dimension increases roughly as the loading of NRS particles increases. A very slight decrease of fractal dimension can be observed when NRS content is increased from 2% to 5% due to the possibly microstructural heterogeneities of the specimens and the variances of MIP test. The augmentation of fractal dimension by layered nano particles was also observed in Ref. [7]. This, to some extent, indicates that NRS particles enhance the complexity of WUHTCC matrix due to the fact that the NRS particles, like other micro admixtures reported elsewhere [33,52,53], possibly act as the foreign fillers to make the matrix more heterogeneous and as the nucleating agents to accelerate or depress the hydration of active binders.

To examine the morphology of the fresh fracture surfaces of WUHTCCs, massive ESEM images in different magnifications were acquired. Generally, there are no obvious differences in micro morphology between the WUHTCC samples, which is consistent with the MIP results discussed above. Due to the limited NRS loadings, it is difficult to figure out the NRS particles in WUHTCC matrix. Here we specially focused on the interactions between fibers and matrix. Fig. 5 shows the typical ESEM pictures of the fibers and/or matrices of WUHTCCs. As is seen, some grooves with the traces of fibers appear in the matrices of WUHTCCs, which is caused by the slip of the fibers during the FPB tests. Matrix can encapsulate fibers with the typical thickness of dense binders within the range of 420 nm to 720 nm; see Fig. 5. This suggests that the interactions between fibers and matrix are relatively weak so the fibers can be pulled out from the matrix. Otherwise, fibers must be broken after the mechanical tests. These relatively weak interactions between

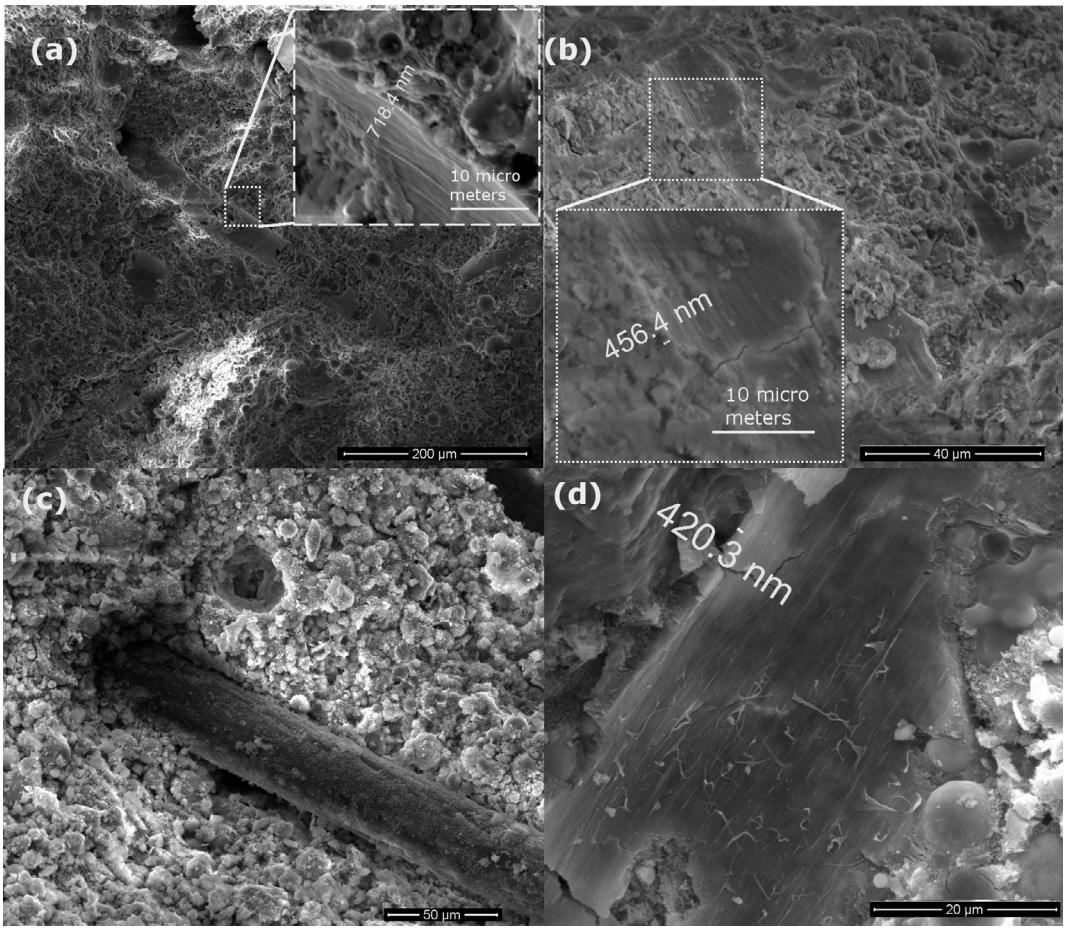

Fig. 5. Typical SEM images of the WUHTCC samples with the different loadings of NRS particles: (a) 0% (WUHTCC-0), (b) 1% (WUHTCC-1), (c) 2% (WUHTCC-2) and (d) 5% (WUHTCC-5).

fibers and matrix are a necessary condition for the strain hardening behaviors of UHTCC [21,28–30]; see the following section for more detailed discussions.

3.2. Mechanical properties

The measured 28-day compressive strengths of cubic WUHTCC specimens with various loadings of NRS particles are shown in Fig. 6; in each case, three WUHTCC specimens were measured and then averaged. As is seen, the compressive strength of WUHTCCs is decreased by around 10% for the material with the low loadings of NRS (WUHTCC-1 and WUHTCC-2), and by more than 20% for the one with 5% NRS (WUHTCC-5). The decrease of compressive strength can be due to the loose pore structure when a cementitious matrix contains hydrophobic NRS particles as depicted in Fig. 4. Furthermore, it has been evidenced that hydrophobic particles can depress hydration, and consequentially cause a slower compressive strength gain of cementitious materials [54]. Although a rapid hardening cement was used in this study, the NRS particles coated with hydrophobic surfactants would lower the compressive strength of WUHTCCs. Similar strength-decreasing effect of hydrophobic admixtures or hydrophobic surface treatments has been well recognized, e.g. [3,55]. Indeed, a premier study by Kuo et al. [14] suggested very slight decreases of compressive strength when the loading of NRS is $\leqslant 5\%$. Later, however, it was reported that the 28-day compressive strength of cement mortars containing 5% NRS particles is 15% higher than that of plain cement mortars [15]. The compression results of cement mortars containing organo-modified montmorillonites showed some fluctuations, but when the particle loading is higher than 1%, compressive strength always decreases [7,8,16,17]. Recent study by Yu et al. [2] showed almost the constant compressive strengths of WUHTCCs with the limited dosages of binders replaced by organically modified nano particles ($< 0.5\%$). The fluctuations of the compressive strength of NRS modified cementitious composites suggest that the effects of NRS particles on the mechanical properties of cementitious composites remain to be advanced. However, compressive strengths higher than 16 MPa (see Fig. 6) make WUHTCC be an appropriate decorating material and even structurally constructing material with the additional function of waterproof.

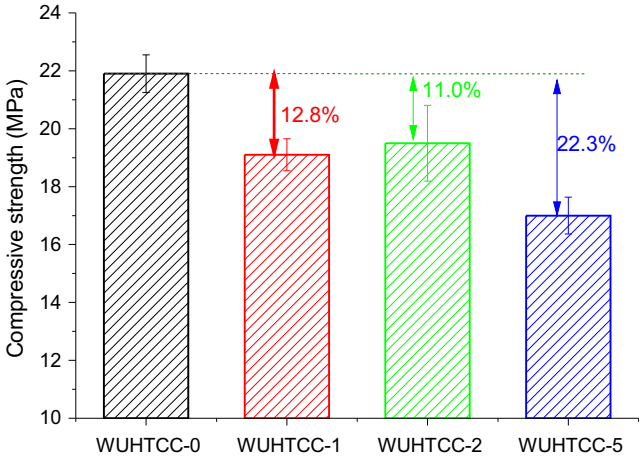

Fig. 6. Average compressive strength of WUHTCCs.

The typical FPB plots of flexural strength versus mid-span deflection for WUHTCCs are displayed in Fig. 7 (left half). Apparently, with the increase of NRS particles, WUHTCCs show better resistance against flexural deformation. The flexural strengths of WUHTCCs increase from 9.64 MPa to 12.73 MPa (by around 30%), while the corresponding maximum deflections show scattering data; see Table 3. A coarse vision examination was performed to assess the cracking patterns of WUHTCCs immediately after the FPB tests. All the WUHTCC specimens show a main tortuous crack and a population of crowded and closely spaced cracks around the main crack; see Fig. 7 (right half).

The geometric characteristics of cracks were evaluated by an image analysis. Fig. 8 shows the cracking patterns of WUHTCCs in the areas of concern. The widths of the main cracks are in the range of 0.6 mm to 3.6 mm. The crowed cracks of WUHTCC-5 are less obvious than those of the other WUHTCC specimens; see Fig. 8(d). The statistic widths of the crowded cracks of WUHTCCs are distributed in the range of 10 to 120 μm with the means size of around 20 μm; see the statistic histograms of the analysed areas displayed in the sub panels of Fig. 8. In addition, all the width distributions of the crowd cracks follow a log-normal type. The log-normal distribution was also reported to capture the air void and pore size distributions of cementitious porous materials [58,57].

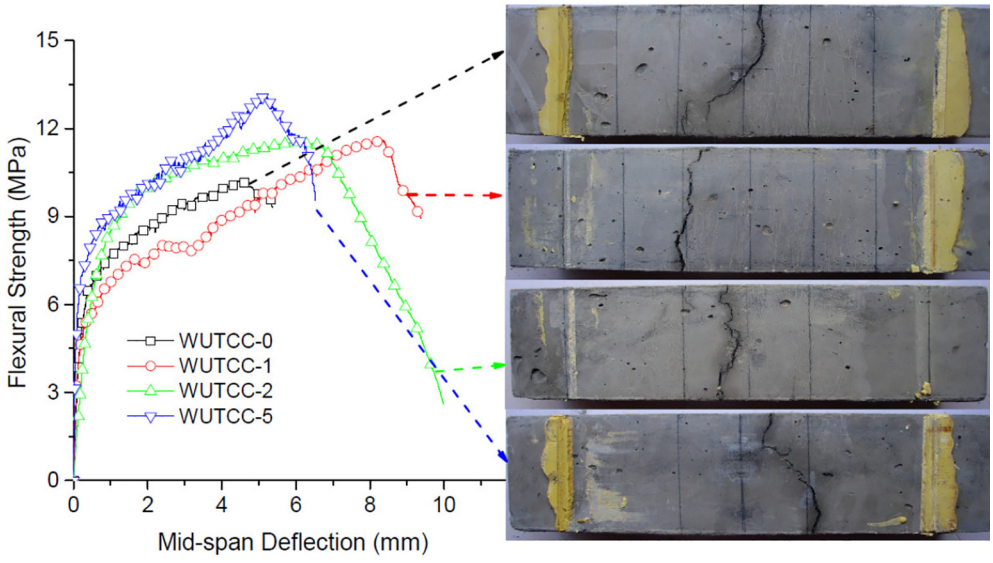

Fig. 7. Typical FPB plots of flexural strength versus mid-span deflection for WUHTCCs (left) and the images of bottom sides after the FPB tests (right).

Table 3
The flexural strength, maximum mid-span deflection and toughness of WUHTCCs.

Sample	Flexural strength (MPa)	Maximum deflection (mm)	Toughness (kJ/m^2)
WUHTCC-0	9.64 ± 0.84	4.30 ± 0.18	37.6
WUHTCC-1	10.70 ± 1.28	7.71 ± 0.87	72.9
WUHTCC-2	11.49 ± 0.10	5.74 ± 0.34	59.5
WUHTCC-5	12.73 ± 0.49	4.75 ± 0.55	53.6

The occurrences of crowded cracks for a WUHTCC during a FPB test cost a large amount of fracture energy, and cause the material to show an excellent toughness [21,28–30]. The flexural toughness of WUHTCCs was estimated from the FPB tests and displayed in Table 3. It shows that the values of toughness are in the range of 38 to 74 kJ/m^2, which are higher than the data of ECCs (15 to 25 J/m^2) reported in Ref. [56]. Considering the fact that the incorporation of NRS particles into cementitious matrix tends to lower the compressive strength as shown in Fig. 6, the maintenance or even enhancement of toughness by the NRS particles may suggest their benefits to the multiple cracking of WUHTCCs under loading.

The flexural characteristics of WUHTCCs displayed in Figs. 7 and 8 come from the delicate balance among the properties of matrix, fibers and fiber/matrix interfaces. Neither the too strong nor the too weak interactions between fibers and matrix can generate the multiple cracking of cementitious composites under loading [21]. The steady state of the multiple cracking in UHTCCs has been proved by numerous experiments [28–30]. While the WUHTCC matrix becomes weaker when NRS particles were used (see the compressive results of Fig. 6), the adhesions between the PVA fibers and the WUHTCC matrix seem to have no obvious changes as displayed in Fig. 5. Therefore, the fibers are always able to sustain the total load and to transfer the load back to the matrix through interfacial shear, and cracks takes place in the matrix. This process may repeat itself, and eventually, creates a population of crowded cracks in the middle span of WUHTCC. However, if the

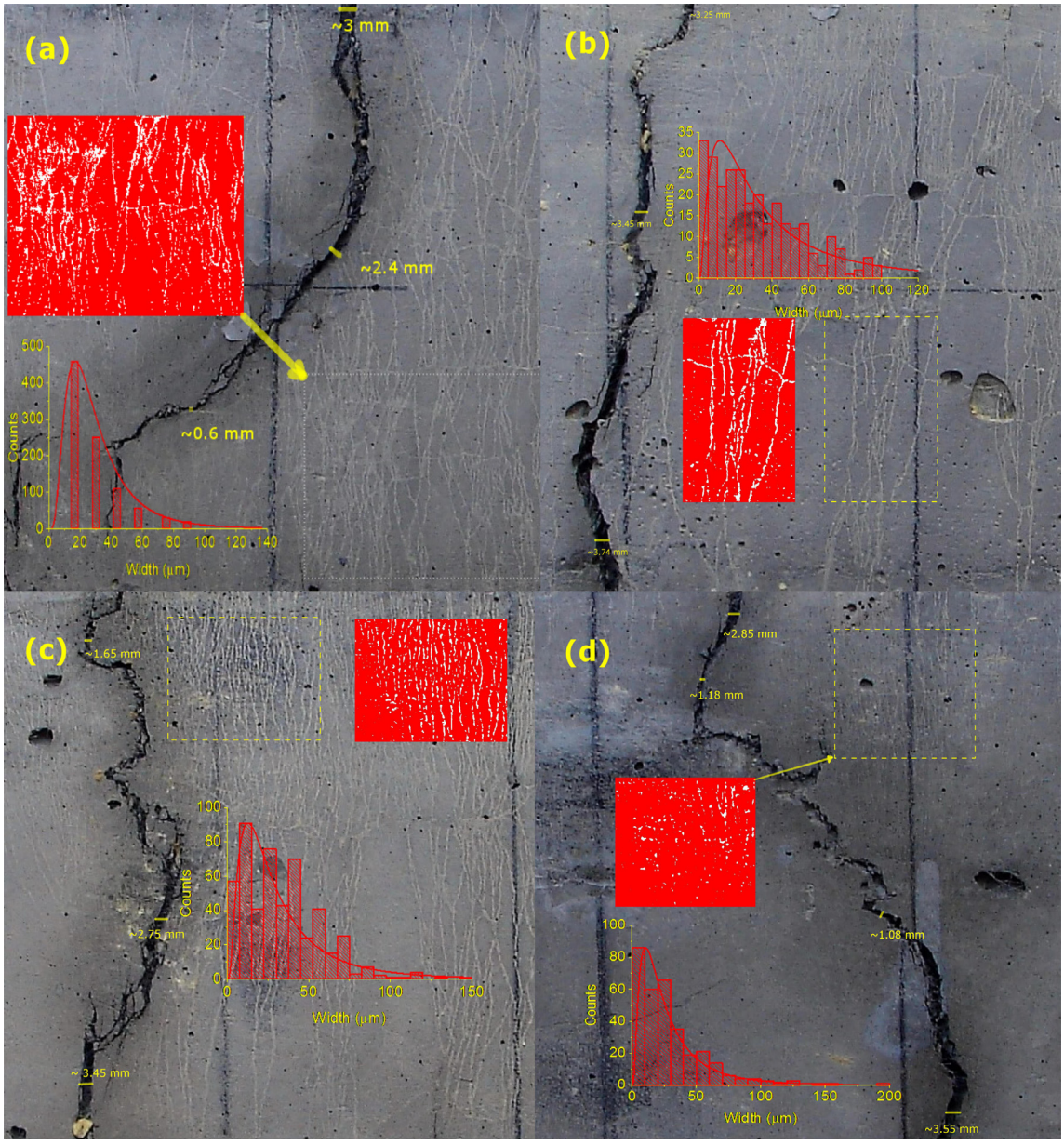

Fig. 8. Cracking patterns of (a) WUHTCC-0, (b) WUHTCC-1, (c) WUHTCC-2 and (d) WUHTCC-5 by imaging analysis.

matrix is too weak, it prefers to form a large crack penetrating through the material. This is why less crowed cracks can be observed for the WUHTCC-5 specimen after the FPB test; see Fig. 8(d). In summary, our study reveals that the incorporation of NRS particles into WUHTCC matrices in a limited loading (< 5%) maintains and/or enhances the multiply cracking and toughness of WUHTCCs.

3.3. Waterproof property

The experiment results of water absorption tests on WUHTCCs with various percentages of NRS particles are shown in Fig. 9. Only 5.8 g water can be absorbed by 100 g dried WUHTCC-0 specimen within 48 h, indicating that the WUHTCC matrix is relatively dense so that water can hardly be absorbed into the material spontaneously. No obvious changes of water absorption take place when 1% NRS particles were added into the binders. However, when the loading of NRS particles is increased to 2% and 5%, the water absorption of WUHTCCs is decreased significantly to 3.2 g and 4.0 g per 100 g dried WUHTCCs, respectively; see Fig. 9(a). By assuming that the volume intruded by mercury at the maximum pressure of a MIP test represents the total pore volume, we can estimate the volume fraction of the water absorbed into the open pores of WUHTCCs to the total pores. It shows that around 28% pore volume can be occupied by water for the WUHTCC-0 and WUHTCC-1 specimens, and only around 16% pore volume for the WUHTCC-2 and WUHTCC-5 ones; see Fig. 9(b). This indicates that the spontaneous absorption of water into the WUHTCC matrix is depressed by the NRS particles. The absorption rates were not tested in this study, but the relevant studies suggested that organically modified nano particles can reduce the absorption rates of WUHTCCs essentially [2].

Fig. 10 shows the experimental results of water penetration tests on WUHTCCs with different loadings of NRS particles. For WUHTCC-0, the maximum survival pressure P_s and the time t_p required to penetrate through the specimens in the thickness of 30 mm are 0.8 MPa and 9 h, respectively. As the loadings of NRS particles increase, both P_s and t_p are increased essentially and continually. For instance, for WUHTCC-5, the P_s and t_p are augmented to 1.5 MPa and 16 h by 87.5% and 77.8%, respectively; see Fig. 10. It indicates that NRS particles enhance the anti-penetration capacity of WUHTCCs remarkably, and akin results are also reported for WUHTCCs [2], cement mortars blended with nano clays [14–17] and self-compacted concrete with nano montmorillonite [59]. As a matter of fact, according to a Chinese standard (GB 50164-2011) [60], both WUHTCC-2 and WUHTCC-5 can be ranked as seepage-resistant concretes.

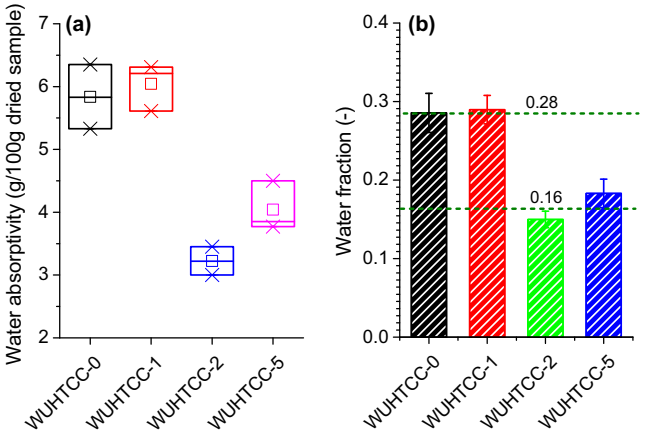

Fig. 9. (a) Statistic results of the water absorption of WUHTCCs by immersing absorption test, and (b) average volume fraction of absorbed water to the total porosity.

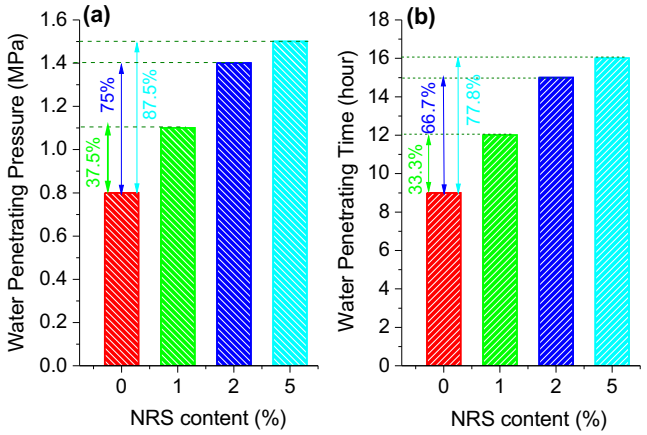

Fig. 10. Water penetration properties of WUHTCCs: (a) the pressure and (b) the time required for water penetrating through the WUHTCC samples.

The observed reductions of absorption and the increases of seepage-resistance are resulted from the coupled effects of microstructure and surface property changed by the incorporation of NRS particles into cementitious matrix. Firstly, NRS particles tune the microstructure of WUHTCC matrix, i.e., inducing more pores in WUHTCCs and enhancing the complexity of cementitous matrix as evidenced by the fractal dimensions presented in Table 2. The increases of porosity and microstructural complexity seem to promote the water absorption by capillary forces [61] but decrease the strength of material as displayed in Fig. 11 and evidenced in the literature [14]. Secondly, the plate-like structure itself may act as a barrier against the penetration of water into the matrix. This barrier comes from the ordered arrayed structures in the cementitious matrix induced by the sheet-like nano particles [59]. Thirdly and more importantly, NRS particles with surface modification tune the surface property of WUHTCC matrix, i.e., increasing the hydrophobicity; see Fig. 11. A study by Kuo et al. [14] indicated that 10% surface-modified NRS particles blended into cementitious binders can increase the contact angles between water drops and substrate from around 10° to more than 60°, which, according to Kelvin equation, lowers the capillary pressure by around 50%, or promotes the seepage-resistance by the same extents. As a result, both the spontaneous water absorption and the forced water penetration of WUHTCC are depressed.

Overall, the relatively high strength and excellent waterproof ability of WUHTCCs provide a way for their extensive uses in the aspects of construction, decoration and repair in the future.

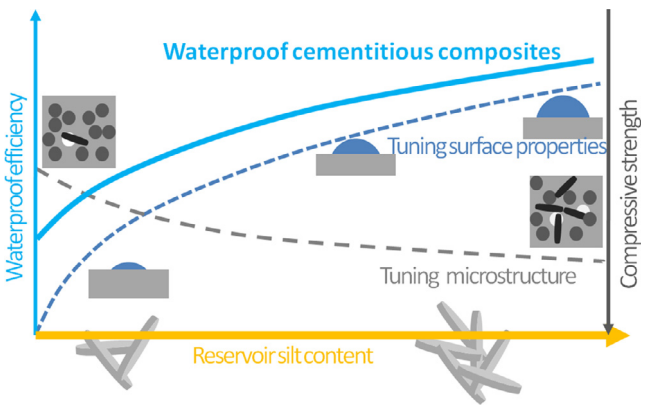

Fig. 11. Mechanisms of waterproof effect by NRS.

4. Conclusions

In the present study, we investigated a type of cementitious composites with the function of waterproof, namely WUHTCCs. By the tests of MIP, strength, FPB, water absorption and penetration, the mechanical properties, micro- and pore structures, waterproof abilities were evaluated and discussed. The obtained results yield the conclusions as follows:

- The porosity of cementitious composites blended with NRS particles increases slightly but the microstructure becomes more complex. The WUHTCCs show similar micro morphology.
- NRS particles tend to decrease the compressive strength of WUHTCCs due to the hydrophobic surfactant, but maintain and even promote their toughness because the multiple cracking of the composites is kept and/or enhanced.
- Both the spontaneous water absorption and the forced water penetration are depressed due to the coupled changes of the microstructure and surface property of WUHTCC matrix by the sheet-like and hydrophobic NRS particles.
- The excellent waterproof property of WUHTCCs facilitates their applications in construction, decoration and repair.

Conflict of interest

The authors declare no competing financial interest.

Author contributions

H. Li and S. Xu designed this study, H. Li conducted the experiments and analysed the results, and Q. Zeng analysed the data and wrote this paper. All authors have given approval to the final version of the manuscript.

Acknowledgement

H. Li and Q. Zeng acknowledge the National Natural Science Foundation of China (Nos. 51478423 and 51408536). The authors thank Prof. Jong-Shin Huang for providing the organo-modified nano reservoir slits and appreciate the efforts of the anonymous reviewers to improve the quality of this study.

References

[1] Y.L. Zheng, M.L. Li, M.Y. Wang, L.D. Yang, Study on influence of seepage of metro tunnels in soft soil on the settlements of tunnels and ground, Chin. J. Geotech. Eng. 27 (2005) 243–247.
[2] J. Yu, H. Li, C.K. Leung, X. Lin, J.Y. Lam, I.M. Sham, K. Shih, Matrix design for waterproof Engineered Cementitious Composites (ECCs), Constr. Build. Mater. 139 (2017) 438–446.
[3] L. Jia, C. Shi, X. Pan, J. Zhang, L. Wu, Effects of inorganic surface treatment on water permeability of cement-based materials, Cem. Concr. Compos. 67 (2016) 85–92.
[4] S. Qiang, K. Chen, Y. Yin, C. Wang, Robust UV-cured superhydrophobic cotton fabric surfaces with self-healing ability, Mater. Design 116 (2017) 395–402.
[5] F.Q. Zhao, H. Li, S.J. Liu, J.B. Chen, Preparation and properties of an environment friendly polymer-modified waterproof mortar, Constr. Build. Mater. 25 (2011) 2635–2638.
[6] B. Wang, S. Xu, F. Liu, Evaluation of tensile bonding strength between UHTCC repair materials and concrete substrate, Constr. Build. Mater. 112 (2016) 595–606.
[7] T.P. Chang, J.Y. Shih, K.M. Yang, T.C. Hsiao, Material properties of Portland cement paste with nano-montmorillonite, J. Mater. Sci. 42 (2007) 7478–7487.
[8] M.A. Kafi, A. Sadeghi-Nik, A. Bahari, A. Sadeghi-Nik, E. Mirshafiei, Microstructural characterization and mechanical properties of cementitious mortar containing montmorillonite nanoparticles, J. Mater. Civ. Eng. 28 (2016) 04016155.
[9] A. Hakamy, F.U.A. Shaikh, I.M. Low, Characteristics of nanoclay and calcined nanoclay-cement nanocomposites, Compos. Part B-Eng. 78 (2015) 174–184.
[10] M.L. Nehdi, Clay in cement-based materials: critical overview of state-of-the-art, Constr. Build. Mater. 51 (2014) 372–382.
[11] M. Aly, M.S.J. Hashmi, A.G. Olabi, M. Messeiry, A.I. Hussain, Effect of nano clay particles on mechanical, thermal and physical behaviours of waste-glass cement mortars, Mater. Sci. Eng. A 528 (2011) 7991–7998.
[12] W. Huang, H. Kazemi-Kamyab, W. Sun, K. Scrivener, Effect of replacement of silica fume with calcined clay on the hydration and microstructural development of eco-UHPFRC, Mater. Des. 121 (2017) 36–46.
[13] Z. Li, J. Gong, S. Du, J. Wu, J. Li, D. Hoffman, X. Shi, Nano-montmorillonite modified foamed paste with a high volume fly ash binder, RSC Adv. 7 (2017) 9803–9812.
[14] W.Y. Kuo, J.S. Huang, T.Z. Tan, Organo-modified reservoir sludge as fine aggregates in cement mortars, Constr. Build. Mater. 21 (2007) 609–615.
[15] W.Y. Kuo, J.S. Huang, Microstructure and properties of cement mortars containing organo-modified reservoir sludge, Constr. Build. Mater. 24 (2010) 2022–2029.
[16] W.Y. Kuo, J.S. Huang, C.H. Lin, Effects of organo-modified montmorillonite on strengths and permeability of cement mortars, Cem. Concr. Res. 36 (2006) 886–895.
[17] W.Y. Kuo, J.S. Huang, B.Y. Yu, Evaluation of strengthening through stress relaxation testing of organo-modified montmorillonite reinforced cement mortars, Constr. Build. Mater. 25 (2011) 2771–2776.
[18] S. Papatzani, Effect of nanosilica and montmorillonite nanoclay particles on cement hydration and microstructure, Mater. Sci. Technol. 32 (2016) 138–153.
[19] Q. Li, X. Gao, S. Xu, Multiple effects of nano-SiO 2 and hybrid fibers on properties of high toughness fiber reinforced cementitious composites with high-volume fly ash, Cem. Concr. Compos. 72 (2016) 201–212.
[20] Q. Li, B. Huang, S. Xu, B. Zhou, C.Y. Rena, Compressive fatigue damage and failure mechanism of fiber reinforced cementitious material with high ductility, Cem. Concr. Res. 90 (2016) 174–183.
[21] V.C. Li, C.K.Y. Leung, Steady-state and multiple cracking of short random fiber composites, J. Eng. Mech. 118 (1992) 2246–2264.
[22] M. Ali, A.M. Soliman, M.L. Nehdi, Hybrid-fiber reinforced engineered cementitious composite under tensile and impact loading, Mater. Des. 117 (2017) 139–149.
[23] A. Hakamy, F.U.A. Shaikh, I.M. Low, Microstructures and mechanical properties of hemp fabric reinforced organoclay cement nanocomposites, Constr. Build. Mater. 49 (2013) 298–307.
[24] A. Hakamy, F.U.A. Shaikh, I.M. Low, Thermal and mechanical properties of NaOH treated hemp fabric and calcined nanoclay-reinforced cement nanocomposites, Mater. Des. 80 (2015) 70–81.
[25] A. Hakamy, F.U.A. Shaikh, I.M. Low, Effect of calcined nanoclay on the durability of NaOH treated hemp fabric-reinforced cement nanocomposites, Mater. Des. 92 (2016) 659–666.
[26] M.S. Morsy, S.H. Alsayed, M. Aqel, Hybrid effect of carbon nanotube and nano-clay on physico-mechanical properties of cement mortar, Constr. Build. Mater. 25 (2011) 145–149.
[27] H. Shoukry, M.F. Kotkata, S.A. Abo-el-Enein, M.S. Morsy, Flexural strength and physical properties of fiber reinforced nano metakaolin cementitious surface compound, Constr. Build. Mater. 43 (2013) 453–460.
[28] H.D. Li, S.L. Xu, Determination of energy consumption in the fracture plane of ultra high toughness cementitious composite with direct tension test, Eng. Frac. Mech. 78 (2011) 1895–1905.
[29] H.D. Li, C.K.Y. Leung, S.L. Xu, Q. Cao, Potential use of strain hardening ECC in permanent formwork with small scale flexural beams, J. Wuhan Univ. Technol. – Mater. Sci. Ed. 24 (2009) 482–487.
[30] H.D. Li, S.L. Xu, C.K.Y. Leung, Tensile and flexural properties of ultra high toughness cemontious composite, J. Wuhan Univ. Technol. – Mater. Sci. Ed. 24 (2009) 677–683.
[31] Standard GB175-2007, Common Portland Cement, National Standard of the People's Republic of China, Beijing (in Chinese).
[32] Q. Zeng, K. Li, T. Fen-Chong, P. Dangla, Pore structure of cement pastes through NAD and MIP analysis, Adv. Cem. Res. 28 (2016) 23–32.
[33] Q. Zeng, K. Li, T. Fen-Chong, P. Dangla, Pore structure characterization of cement pastes blended with high-volume fly-ash, Cem. Concr. Res. 42 (2012) 194–204.
[34] Q. Zeng, K. Li, T. Fen-Chong, P. Dangla, Analysis of pore structure, contact angle and pore entrapment of blended cement pastes from mercury porosimetry data, Cem. Concr. Compos. 34 (2012) 1053–1060.
[35] Q. Zeng, H. Sun, D. Zhang, K. Li, Characterizing pore structure of the blended cement pastes using water vapor sorption isotherms, Mater. Charact. 95 (2014) 72–84.
[36] Q. Zeng, K. Li, Reaction and microstructure of cement–fly-ash system, Mater. Struct. 48 (2015) 1703–1716.
[37] C.A. Schneider, W.S. Rasband, K.W. Eliceiri, NIH Image to ImageJ: 25 years of image analysis, Nat. Methods 9 (2012) 671–675.
[38] Z. Wang, Q. Zeng, L. Wang, K. Li, S. Xu, Y. Yao, Characterizing frost damages of concrete with flatbed scanner, Constr. Build. Mater. 102 (2016) 872–883.
[39] H.S. Chen, L.J. Sluys, P. Stroeven, W. Sun, Theoretical prediction on thickness distribution of cement paste among neighboring aggregates in concrete, Comput. Concr. 8 (2011) 163–176.
[40] Standard DL/T 5126-2001, Polymer Modified Cement Mortar Testing Criteria, China Electric Power Publishing House, Beijing, 2001 (in Chinese).
[41] ASTM-C1585, Standard Test Method for Measurement of Rate of Absorption of Water by Hydraulic-Cement Concretes. C1585-13. ASTM International, West Conshohocken, PA, USA, 2013.
[42] Standard JGJ/T 70-2009, Standard Test Method for Performance of Building Mortar, China Ministry of Construction, Beijing, 2009 (in Chinese).

[43] R. Wang, P. Wang, Function of styrene-acrylic ester copolymer latex in cement mortar, Mater. Struct. 43 (2010) 443–451.
[44] C.A.L. y Leon, New perspectives in mercury porosimetry, Adv. Colloid Interface Sci. 76 (1998) 341–372.
[45] Q. Zeng, K. Li, T. Fen-Chong, P. Dangla, Effect of porosity on thermal expansion coefficient of cement pastes and mortars, Constr. Build. Mater. 28 (2012) 468–475.
[46] J.J. Thomas, H.M. Jennings, A colloidal interpretation of chemical aging of the CSH gel and its effects on the properties of cement paste, Cem. Concr. Res. 36 (2006) 30–38.
[47] A.J. Allen, J.J. Thomas, H.M. Jennings, Composition and density of nanoscale calcium silicate hydrate in cement, Nat. Mater. 6 (2007) 311–316.
[48] Q. Zeng, K. Li, T. Fen-Chong, P. Dangla, Surface fractal analysis of pore structure of high-volume fly-ash cement pastes, Appl. Surf. Sci. 257 (2010) 762–768.
[49] Q. Zeng, M. Luo, X. Pang, L. Li, K. Li, Surface fractal dimension: an indicator to characterize the microstructure of cement-based porous materials, Appl. Surf. Sci. 282 (2013) 302–307.
[50] K. Li, Q. Zeng, M. Luo, X. Pang, Effect of self-desiccation on the pore structure of paste and mortar incorporating 70% GGBS, Constr. Build. Mater. 51 (2014) 329–337.
[51] Q. Li, S. Xu, Q. Zeng, The effect of water saturation degree on the electrical properties of cement-based porous material, Cem. Concr. Compos. 70 (2016) 35–47.
[52] W. Meng, P. Lunkad, A. Kumar, K. Khayat, Influence of silica fume and polycarboxylate ether dispersant on hydration mechanisms of cement, J. Phys. Chem. C 120 (2016) 26814–26823.
[53] Q. Zeng, K. Li, T. Fen-Chong, P. Dangla, Determination of cement hydration and pozzolanic reaction extents for fly-ash cement pastes, Constr. Build. Mater. 27 (2012) 560–569.
[54] P. Hosseini, R. Hosseinpourpia, A. Pajum, M.M. Khodavirdi, H. Izadi, A. Vaezi, Effect of nano-particles and aminosilane interaction on the performances of cement-based composites: an experimental study, Constr. Build. Mater. 66 (2014) 113–124.
[55] F. Tittarelli, G. Moriconi, The effect of silane-based hydrophobic admixture on corrosion of reinforcing steel in concrete, Cem. Concr. Res. 38 (2008) 1354–1357.
[56] V.C. Li, T. Hashida, Engineering ductile fracture in brittle-matrix composites, J. Mater. Sci. Lett. 12 (12) (1993) 898–901.
[57] Q. Zeng, L. Li, X. Pang, Q. Gui, K. Li, Freeze thaw behavior of air entrained cement paste saturated with 10 wt.% NaCl solution, Cold Reg. Sci. Technol. 102 (2014) 21–31.
[58] Q. Zeng, T. Fen-Chong, K. Li, Freezing behavior of cement pastes saturated with NaCl solution, Constr. Build. Mater. 59 (2014) 99–110.
[59] P. Hosseini, A. Afshar, B. Vafaei, A. Booshehrian, A. Esrafili, Effects of nano-clay particles on the short-term properties of self-compacting concrete, Eur. J. Environ. Civ. Eng. 21 (2017) 127–147.
[60] GB 50164-2011, Standard for Quality Control of Concrete, China Ministry of Construction, Beijing, 2011 (in Chinese).
[61] J. Cai, E. Perfect, C.L. Cheng, X. Hu, Generalized modeling of spontaneous imbibition based on Hagen Poiseuille flow in tortuous capillaries with variably shaped apertures, Langmuir 30 (2014) 5142–5151.